Food Control 70 (2016) 229–241

Contents lists available at ScienceDirect

Food Control

journal homepage: www.elsevier.com/locate/foodcont

Non-destructive detection of blackspot in potatoes by Vis-NIR and SWIR hyperspectral imaging

Ainara López-Maestresalas [a], Janos C. Keresztes [b], Mohammad Goodarzi [b], Silvia Arazuri [a], Carmen Jarén [a], Wouter Saeys [b, *]

[a] Department of Agricultural Projects and Engineering, Universidad Pública de Navarra, Campus de Arrosadia, 31006, Navarra, Spain
[b] KU Leuven Department of Biosystems, MeBioS, Kasteelpark Arenberg 30, 3001, Leuven, Belgium

ARTICLE INFO

Article history:
Received 18 April 2016
Received in revised form
31 May 2016
Accepted 1 June 2016
Available online 2 June 2016

Keywords:
Vis-NIR
SWIR
Hyperspectral imaging
Solanum tuberosum L.
Potato
Blackspot

ABSTRACT

Blackspot is a subsurface potato damage resulting from impacts during harvesting. This type of bruising represents substantial economic losses every year. As the tubers do not show external symptoms, bruise detection in potatoes is not straightforward. Therefore, a nondestructive and accurate method capable of identifying bruised tubers is needed. Hyperspectral imaging (HSI) has been shown to be able to detect other subsurface defects such as bruises in apples. This method is nondestructive, fast and can be fully automated. Therefore, its potential for non-destructive detection of blackspot in potatoes has been investigated in this study. Two HSI setups were used, one ranging from 400 to 1000 nm, named Visible-Near Infrared (Vis-NIR) and another covering the 1000–2500 nm range, called Short Wave Infrared (SWIR). 188 samples belonging to 3 different varieties were divided in two groups. Bruises were manually induced and samples were analyzed 1, 5, 9 and 24 h after bruising. PCA, SIMCA and PLS-DA were used to build classifiers. The PLS-DA model performed better than SIMCA, achieving an overall correct classification rate above 94% for both hyperspectral setups. Furthermore, more accurate results were obtained with the SWIR setup at the tuber level (98.56 vs. 95.46% CC), allowing the identification of early bruises within 5 h after bruising. Moreover, the pixel based PLS- DA model achieved better results in the SWIR setup in terms of correctly classified samples (93.71 vs. 90.82% CC) suggesting that it is possible to detect blackspot areas in each potato tuber with high accuracy.

1. Introduction

According to the FAO (Food and Agriculture Organization of the United Nations), worldwide potato production was above 360 million tons in 2013 (FAO, 2014). So, potato is a major food crop for which it is essential to ensure food quality along the potato supply chain (López, Arazuri, García, Mangado, & Jarén, 2013).

Blackspot bruise in potato (*Solanum tuberosum* L.) is an internal damage mainly produced from impacts either between the tubers and hard surfaces or between each other during mechanical harvesting and subsequent handling (Boeriu, Yuksel, Van der Vuurst de Vries, Stolle-Smits, & Van Dijk, 1998; Fluck & Ahmed, 1973; Mathew & Hyde, 1997). This type of bruise appears at the sub-surface and most frequently at the stem end of the tubers due to the fact that the radius of curvature is smaller there (Sawyer & Collin, 1960). The resulting blue-black discoloration of the damaged tissue is a consequence of oxidation of tyrosine by polyphenol oxidase (Dean, Jackowiak, Nagle, Pavek, & Corsini, 1993; Fluck & Ahmed, 1973). The damaged tissue tends to absorb more oil during frying (Baritelle, Hyde, Thornton, & Bajema, 2000), resulting in after-cooking darkening, one of the most undesirable effects reported by consumers (Wang-Pruski & Nowak, 2004).

The economic losses in the fruit and vegetable industry related to bruising are considerable (Van Zeebroeck et al., 2003). According to Peters (1996), in the American potato industry, bruising represents substantial economic losses every year and 70% of total damage is caused by harvesting. Mathew and Hyde (1997), reported an estimated $20 to $60 million losses due to potato tuber bruising in the Washington State, the second major potato producer in the US, in a particularly bad year.

An important factor contributing to the financial loss is the fact that the affected tubers do not show external damage and are, therefore, processed as healthy ones, resulting in a waste and loss of

* Corresponding author.
E-mail address: Wouter.saeys@biw.kuleuven.be (W. Saeys).

http://dx.doi.org/10.1016/j.foodcont.2016.06.001
0956-7135/

confidence among consumers (Evans & Muir, 1999). However, the detection of those affected tubers, would allow those potatoes to be assigned to other uses like fourth range products, where tubers are processed and commercialized generally peeled and cut avoiding the use of damage areas.

In the past, damage in potatoes was assessed using catechol dye. Catechol reacts with exposed starch and discolours the surface areas with external damage (O'Leary & Iritani, 1969). This method was not suitable for blackspot determination since this type of damage occurs at the subsurface of the tubers without exposing starch. For this, tetrazolium, a chemical capable of identifying blackspot bruising, was used. However, both products were later known to be toxic to animals while tetrazolium was also toxic to humans (Kleinschmidt & Thornton, 1991) and therefore, they are no longer used.

Different protocols have been used in order to test tuber damage at either harvest or packaging. Since some types of bruises can take long to become visible (two to four days), the use of a hot box is a recommended option as it speeds up bruising development allowing damages to be visible within six to 12 h (Thornton & Bohl, 1998).

In a report published by Jack, Dessureault, and Prasad (2013) damage of potatoes in a real washing and packaging line was identified. To this end, they collected 42 samples of potatoes from 4 to 3 different points along the washing and packaging line, respectively, and placed them in a hot box for a minimum of 12 h with the temperature set to 35 °C. After that period, tubers were washed gently to remove dirt and visually assessed after peeling. They found that 10 ± 8% of the tubers presented some kind of damage at the washing line, while a notably higher proportion of the samples (52% ± 30%) were damaged in the packaging line. These numbers highlight the need for a non-destructive technique to detect this internal damage before tubers reach the market, in order to reduce the current losses and regain customers' trust.

Hyperspectral imaging, a technique combining the principles of spectroscopy and imaging, has been applied to subsurface defect detection in fruit and vegetables, such as apples (ElMasry, Wang, Vigneault, Qiao, & ElSayed, 2008; Lu, 2003; Xing & De Baerdemaeker, 2005; Xing, Saeys, & De Baerdemaeker, 2007), pears (Zhao, Ouyang, Chen, & Wang, 2010) and mushrooms (Gowen et al., 2008). In the case of potatoes the usefulness of hyperspectral imaging has been reported for the discrimination between potato tubers and clods (Hägg, Häkkinen, Kumpulainen, Ahvenainen, & Hurme, 1998; Vanderslice, Higgs, Hayes, & Block, 1990), the detection of hollow heart (Dacal-Nieto, Formella, Carrión, Vazquez-Fernandez, & Fernández-Delgado, 2011b) and the detection of common scab (Dacal-Nieto, Formella, Carrión, Vazquez-Fernandez, & Fernández-Delgado, 2011a). Thybo, Jespersen, Lærke, and Stødkilde-Jørgensen (2004) were able to identify internal bruises in potato slices of cultivar Saturna by applying magnetic resonance imaging. Rady and Guyer (2015) recently reviewed the state of the art in non-destructive quality evaluation of potatoes from the first application in the sixties up to now. However, no reports were found on the non-destructive detection of blackspot damage in intact potatoes.

Considering the promising results reported for hyperspectral imaging techniques in identifying subsurface defects in different fruit and vegetables and other potato defects, the objective of this study was to evaluate the potential of hyperspectral imaging for blackspot detection in potatoes. Two wavelength regions of the electromagnetic spectrum were considered: Visible-Near Infrared (Vis-NIR, 400–1000 nm) and Short Wave Infrared (SWIR, 1000–2500 nm).

2. Material and methods

2.1. Sample preparation

A total of 188 potato tubers of three different cultivars (Hermes, Bintje and Magnum) harvested in 2013 were analyzed in this study. Samples from cv. Hermes (109 tubers) were provided by The Basque Institute for Agricultural Research and Development (NEIKER-Tecnalia), Spain and were sent to KU Leuven Department of Biosystems, MeBioS, Leuven, Belgium, for the measurements. Samples from cv. Bintje and Magnum, consisting of respectively 44 and 35 tubers, were supplied by a local farmer in Leuven, Belgium. The tubers were randomly divided in two groups of equal size. The potatoes of the first group ($n_b = 94$) were subjected to impact in order to induce internal bruising, while the others ($n_h = 94$) served as the control group. Prior to analysis samples were kept in a refrigerator at 4 °C. Then, samples were washed and weighted.

In order to induce the bruises, the tubers were dropped 300 mm inside a cylinder above an impactor facing the stem end (Fig. 1). They were left to fall free and hit a hemispherical head of 25 mm in diameter attached to a circular flat plate. The calculated impact energy varied between 303 mJ and 994 mJ depending on the mass of the potatoes. After impact, tubers were kept in a hot climate

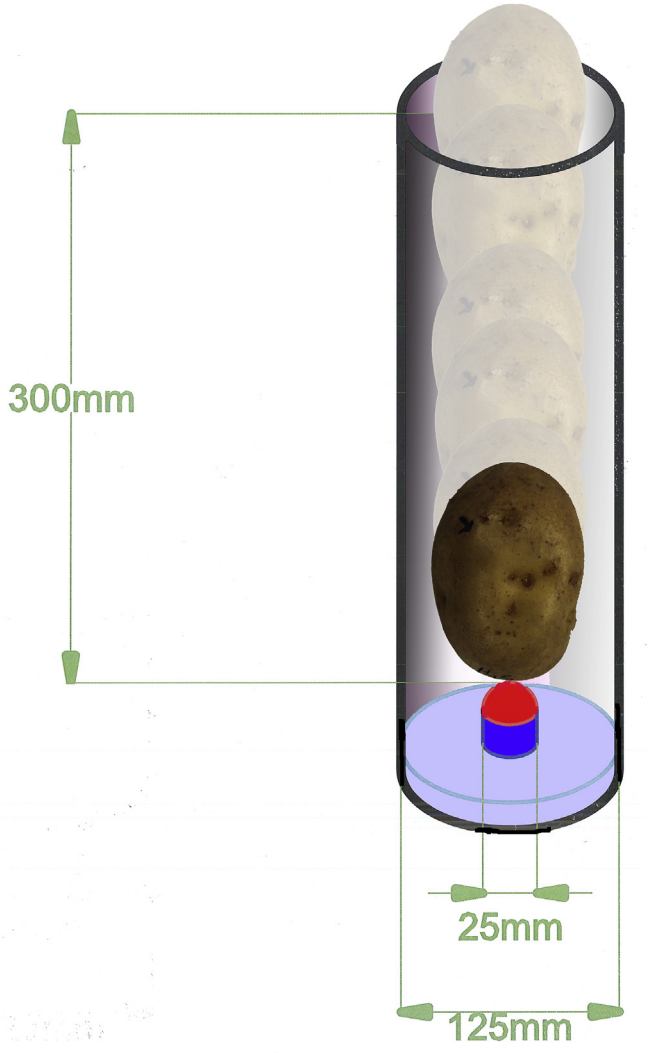

Fig. 1. Schematic diagram of the system used to induce bruises.

control chamber (Weiss WKL 100, Weiss Umwelttechnik GmbH, Reiskirchen-Lindenstruth, Germany) at a temperature of 34 °C with 95% relative humidity for 24 h, because combination of both high temperature and high humidity has been reported to promote a faster development of the bruises (Wang-Pruski & Nowak, 2004).

Samples were then scanned with the hyperspectral imaging system 1, 5, 9 and 24 h after the impacts, as will be explained in the following section. All the samples were placed with the stem end facing the hyperspectral imaging system. After all measurements, samples were peeled and photographed with a standard RGB camera (Powershot 1100D, Canon Corporation, Japan) to check whether the healthy ones already had bruises and the bruise-induced ones had developed them or not.

Samples were divided into 2 classes for statistical analysis. Class 1 ($n_{C1} = 94$) corresponding to the Healthy group and Class 2 ($n_{C2} = 376$) including bruised samples measured at the different times after bruising: 1 h group, 5 h, 9 h and 24 h. Each group containing 94 samples.

2.2. Hyperspectral imaging

The hyperspectral imaging was performed at the KU Leuven Department of Biosystems, MeBioS, Leuven, Belgium. Potato samples were scanned on a setup for hyperspectral imaging that consists of: a transportation plate, an illumination unit, two hyperspectral cameras (one for the Vis-NIR range from 400 to 1000 nm and one for the SWIR range from 1000 to 2500 nm) and a computer. The Vis-NIR hyperspectral camera used in this study consists of a CCD camera (TXG14, Baumer, Germany) with a 1392 by 1040 pixel image resolution coupled to a prism-grating-prism-based imaging spectrograph (ImSpector V10, Spectral Imaging Ltd., Oulu, Finland), and a focusing lens (Canon TV Lens, VF 25 mm, f/0.95, Japan). The SWIR hyperspectral camera (HS SWIR XS-M320C4-60, Headwall Photonics Inc., Fitchburg, MA) consists of an MCT camera (XEVA MCT-2140, Xenics, Leuven, Belgium) with a 320 by 256 pixel resolution with a reflective concentric grating (HS SWIR XS-M320C4, Headwall Photonics Inc., Fitchburg, MA), a slit of 60 μm, and a focusing lens (Oles 22.5, Specim Ltd, Oulu, Finland) with a focal length of 22.5 mm. Both hyperspectral cameras are pushbroom instruments (also called line-scan instrument). These instruments scan a single line at a time for which the light is split into its wavelength components and projected onto the camera chip. In this way, images with a spatial and a spectral dimension are recorded. To scan the entire sample line by line a transportation unit is required to move the samples under the line-scan camera. The transportation plate used in this research was a computer controlled translation stage (TLA 15-400, Franke GmbH, Aalen, Germany). Six halogen lamps (DECOSTAR ALU 12 V-20 W-36°, OSRAM, Germany) were used to illuminate the samples. Four of them were arranged on an arc frame, while the other two were set one at the front of the sample and another at the back of it to achieve homogeneous illumination of the scanned area (Fig. 2). The entire setup was controlled by a computer equipped with LabView V8.5 software (National Instruments, Austin, TX).

The exposure time was optimized at 35 ms and 2 ms for the Vis–NIR and SWIR cameras, respectively, in order to maximize the spectral signal to noise ratio while avoiding saturation of specular reflective regions. The translation stage speed was set to 100 mm/s and 200 mm/s and images were captured consequently in intervals of 0.3 mm and 0.1 mm for the Vis–NIR and SWIR cameras, respectively.

2.2.1. Reflectance calibration

Three images were acquired for the reflectance calibration with both the Vis-NIR and SWIR cameras. First, white reference measurements (W) were obtained using a white calibration tile for both the Vis-NIR and SWIR range (Spectralon® Reflectance Standards 75%, RSS-08-010, Labsphere, North Sutton, USA). Dark references (D) were acquired every 1, 5, 9 and 24 h with the illumination switched off and the camera lens covered by a cap. Finally, all images of samples (S) were first scanned with one spectral range at each time (1, 5, 9 and 24 h) and then with the other. The following equation was used to convert the raw intensity values in the hyperspectral images into relative reflectance values:

$$R = \frac{I_S - I_D}{I_W - I_D} \quad (1)$$

where, R is the relative reflectance, I_S corresponds to the intensity value acquired on the sample, I_D is the intensity acquired for the dark reference and I_W is the intensity acquired on the white reference tile.

2.2.2. Segmentation

The first step in image segmentation consists in separating the region of interest, namely the potato, from the background. In this study, all potato images were processed and analyzed individually using the following procedure: Two masks were applied to remove the background and the saturated pixels in each image, as these pixels do not contain any information on the quality of the tubers. It should be noted here that no specular reflections were observed on the bruised areas. To remove the background in the Vis-NIR reflectance hypercubes a threshold of 0.10 was applied to the reflectance image at 854 nm, while a threshold of 0.09 was applied to the reflectance image at 1106 nm for the SWIR hypercube. All pixels with values below those thresholds were labelled as background. Then, a high mask was applied to select saturated pixels by thresholding at values of 0.55 and 0.57 for Vis-NIR and SWIR, respectively, to produce a binary image of saturated pixels only. In this study, the entire potato, except for the saturated pixels, was defined as the region of interest (ROI). This region of interest was then used to calculate the mean spectrum of each potato to be used in the future analyses. In Fig. 3 the steps followed for detection of potatoes affected by blackspot once the images were captured using both hyperspectral setups are schematically illustrated.

2.3. Multivariate data analysis

Data pre-processing and classification modeling were performed in MATLAB R2014a (The MathWorks, Natick, MA) using the PLS_Toolbox (Eigenvector Research Inc., Wenatchee, WA).

2.3.1. Spectral pre-processing techniques

Pre-processing or pre-treatment methods are commonly used to reduce or avoid the influence of unwanted effects in the data such as light scattering (Brown, Culley, Yang, Durst, & Wrolstad, 2005). Since these effects can negatively affect the reliability of the multivariate model (Barbin, ElMasry, Sun, & Allen, 2012), pre-processing techniques must be applied prior to model building. The techniques which have shown to be effective in classical spectroscopy are also frequently applied to hyperspectral imaging data (Vidal & Amigo, 2012). The principal spectral pre-processing techniques are smoothing, derivatives and scatter correction.

The smoothing technique allows to remove some of the instrumental noise. Among the different algorithms available, Savitzky-Golay (SG) is the most popular for this purpose (Brown et al., 2005).

Both standard normal variate (SNV) and Multiplicative Scatter Correction (MSC) are techniques capable of reducing the effects of light scattering on the acquired spectra (Rinnan, Berg, & Engelsen,

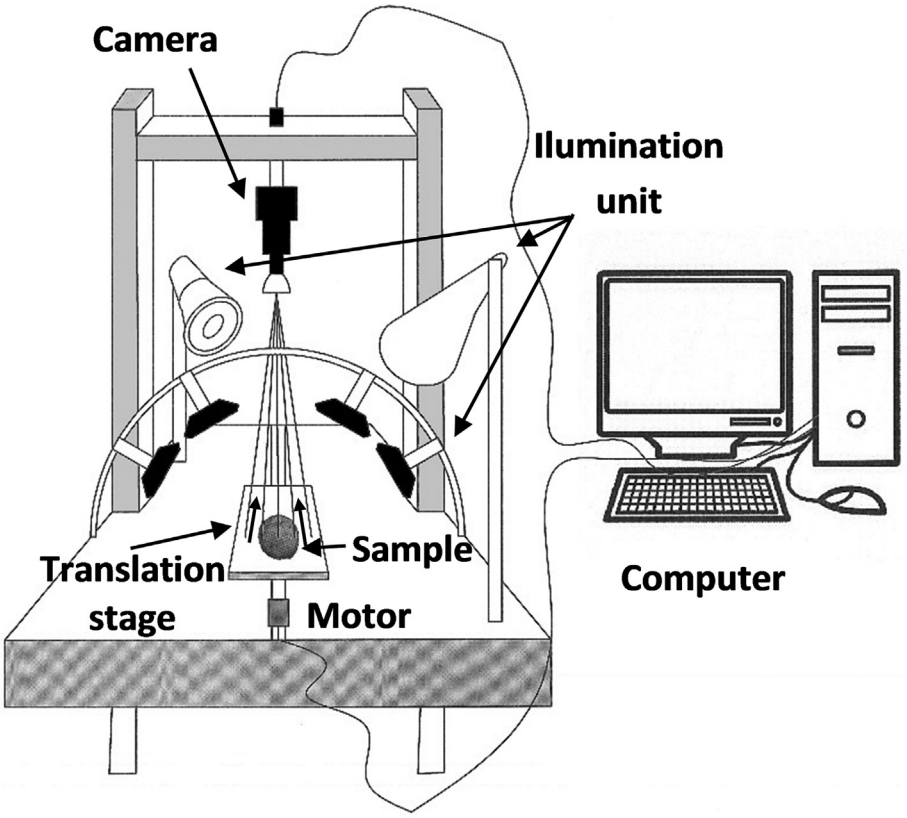

Fig. 2. Schematic diagram of the hyperspectral imaging system used for potato scanning.

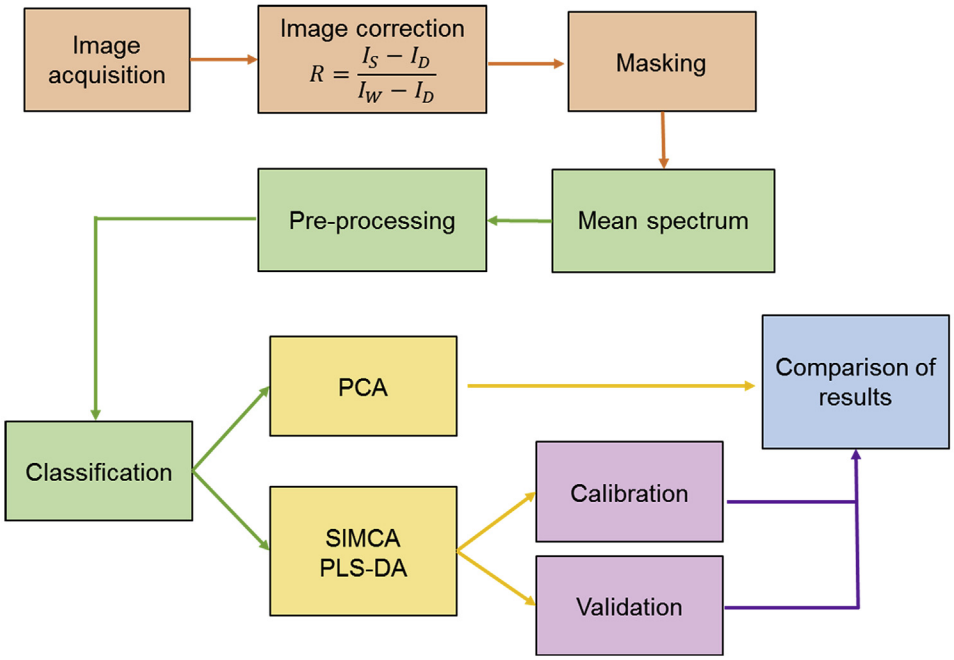

Fig. 3. Flowchart for potato internal quality detection using hyperspectral imaging.

2009), which typically provide similar results. SNV is a method of spectral normalization, which establishes a common scale for all spectra by centering each spectrum around its mean value and scaling it by its standard deviation. In this way, it corrects for additive and multiplicative variation between spectra. MSC estimates the multiplicative and additive effects within a set of data by regressing each spectrum onto a reference spectrum, which is typically the mean spectrum. The spectrum is then pre-processed

by subtracting the estimated intercept value and dividing by the estimated slope value (Dhanoa, Lister, Sanderson, & Barnes, 1995).

As for derivative transformations, both first and second derivatives remove baseline offsets in the data, while the latter is also useful for separating overlapping peaks (Burger & Geladi, 2007).

In this study, before any other pre-treatment, each mean spectrum of every sample was smoothed by a 15 points Savitzky-Golay filtering operation. Then, different combinations of the methods described above were used for model building. The effect of no pre-treatment at all was also analyzed. 1st (D1) and 2nd (D2) derivatives by Savitzky-Golay (SG) method were calculated by second order polynomial and 15 window points. Finally, all pre-treated data, as well as the non pre-treated data, were mean-centered (MC) to reduce the systematic noise (Barbin et al., 2012).

The cross-validation (CV) method chosen was Venetian Blinds with 10 data subsets (splits). In this type of CV, each test set is determined by selecting every *s*th object in the data set, starting at objects numbered 1 through *s*.

2.3.2. Unsupervised analysis (PCA)

Principal Component Analysis (PCA) was used in the first place to understand the data by analyzing the differences which exist between the samples and identifying possible outliers as well as to visualize any possible segregation or clustering among different classes. This is a method able to extract the main sources of variability in the data (Kotikova et al., 2007). It transforms the variables into Principal Components (PCs) which are linear combinations of the spectral data which describe most of the variation in the original variables (Kamruzzaman, Barbin, ElMasry, Sun, & Allen, 2012). The first PC is defined as the linear combination of the original variables which captures the largest part of the variation in the data, the second captures as much as possible variation orthogonal to the first PC, and so on (Barker & Rayens, 2003). In this study, the ability of PCA to separate the different groups was examined visually by inspecting the scores plots.

2.3.3. Soft Independent Modeling of Class Analogy (SIMCA)

Soft Independent Modeling of Class Analogy (SIMCA) is a supervised classification technique that has been successfully applied to solve many pattern recognition problems (Massart, Vandeginste, Deming, Michotte, & Kaufman, 1988). Being a supervised method, SIMCA requires knowledge on the Class membership of the samples in the training set. Therefore, a classification model is built by using a training data set of samples with known Class affiliation and is then evaluated using external samples (Martens & Naes, 1989). In SIMCA, a separate PCA model is built for each class. Samples are projected onto the different PCA models and a metric is used which combines the distance from the model (Q-residual) with the distance from the centre of the model within the model (Hotelling T^2) in order to calculate Class membership. As a consequence, it is theoretically possible that samples are classified in multiple classes or in none.

2.3.4. Partial Least Squares Discriminant Analysis (PLS-DA)

Partial Least Squares Discriminant Analysis (PLS-DA) is a pattern recognition technique where the Class memberships are predicted from the sample spectra by means of PLS regression (Höskuldsson, 1988; Wold, 1966). In PLS regression, orthogonal linear combinations of the original variables are defined which maximally capture the covariance between the X and Y variables. These linear combinations are referred to as Latent Variables (LVs) or PLS components. In order to be able to use Partial Least Squares Regression (PLSR) for discrimination purposes, the Class variable must be transformed into a binary-coded dummy matrix with the same number of rows as X and the same number of columns as there are Classes. Thus, the first column of Y will be a vector with all values equal to zero except for the samples belonging to the first category where it will be equal to 1. Then, in the same way as for the regression method, the model will give a calculated Y that will not have either 1 or 0 values perfectly. So, a threshold has to be defined to decide if an object is assigned to the category or not (Ballabio & Todeschini, 2009).

In this study, a 2 column response matrix **Y** was introduced in which samples belonging to the first Class (Healthy) were described by the dependent vector **[1 0]** and likewise, samples belonging to the second (Bruised), by the vector **[0 1]**.

2.3.5. Blackspot detection

Also in our study, the ability of Vis-NIR and SWIR hyperspectral systems to detect blackspot areas in each potato tuber was investigated. This was performed with the objective to use a detector capable of mapping out the sound areas and the blackspot affected ones for each potato (each hypercube) at the final stage of the potato manufacturing process. In order to develop this mapping, each pixel of the hypercube is individually classified (is taken as one sample) in the PLS-DA model. Then, with the results of this classification model, a map of the affected areas in each tuber is created.

With that aim, 10 and 5 potatoes belonging to Bruised Class and analyzed 24 h after impacts were selected as the calibration and external validation set, respectively. Same tubers were selected for both hyperspectral ranges. That selection was made in accordance with the results obtained in the PLSDA based on the mean spectrum where the clearest discrimination results were obtained for the 24 h group of samples.

In this study, the function roipoly (region inside a polygon) MATLAB function (MATLAB, Version. “8.3. 0.532 (R2014a) The MathWorks, Natick, MA) was applied to each tuber to manually select a polygonal ROI within the image corresponding to the bruised area. After selection of the desired ROI, this function creates a mask with the same size as the roipoly. The roipoly consists of a binary image with 1 and 0 inside or outside the polygon. In our study, that binary image was then selected as the bruised mask. Finally, the resulting product from the subtraction between the whole mask and the bruised mask was selected as the healthy mask.

Since that selection led to a large number of pixels, the Kennard and Stone (KS) algorithm was applied to select a representative number of the pixels in each mask (Xing & De Baerdemaeker, 2005). This algorithm has recently been successfully applied for pixel selection in NIR spectroscopy (Casale, Casolino, Oliveri, & Forina, 2010; Hesen & Kroesbergen, 1960) and hyperspectral imaging (Kennard & Stone, 1969; Riccioli, Pérez-Marín, Guerrero-Ginel, Saeys, & Garrido-Varo, 2011). In this work, the KS algorithm was applied to select half of the pixels in both Classes (Healthy and Bruised) in the Vis-NIR and SWIR spectral ranges. The resulted data matrix after applying the KS algorithm consisted of 463,995 rows and 220 columns in which the healthy area was represented by 452,622 rows and the bruised area by the remaining 11,373 rows in the Vis-NIR spectral range. This data matrix was comprised by 10 potatoes and used as the training set. Accordingly, the test set consisted of 5 potatoes individually analyzed representing an overall data matrix of 178,560 rows and 220 columns, where the Healthy Class accounted for 175,029 rows and the Bruised Class for the remaining 3531 rows.

In the same terms, after applying KS algorithm to the SWIR spectral data, the resulting data matrix represented by 10 tubers and used as the training set consisted of 269,938 rows and 150 columns, where the Healthy Class covered 263,094 rows and the remaining 6844 were covered by the Bruised Class. Consequently,

the test set represented by 5 tubers accounted for a total data matrix of 114,410, in which the Healthy Class represented a total of 107,921 rows while Bruised Class covered 1893 rows.

2.3.6. Model validation and accuracy

In this study, for the supervised classification methods (SIMCA and PLS-DA), potato samples were randomly divided into training and test sets consisting of respectively 70% and 30% of the tubers. Only the training data set was used to build the classification model, while the test data set was used to test its capability of classifying new samples.

The comparison between the two spectral ranges used and different pre-processing techniques was based on the overall accuracy of the classification model in the training and test sets. This accuracy was determined by the percentage of correctly classified (% CC) samples and the sensitivity and specificity of each Class for both SIMCA and PLS-DA classification techniques.

For each Class A, the sensitivity is defined as the proportion of samples belonging to that Class A that are correctly classified (True positives (TP)). Similarly, the proportion of samples belonging to another Class B which are classified as Class A, are named False positives (FP). The specificity for the same Class A corresponds to the proportion of samples belonging to another Class B that are correctly classified as Class B (True negatives (TN)) and, finally, the False negatives (FN) are those samples belonging to Class A which are falsely classified as Class B. These parameters can be written as follows (Parikh, Mathai, Parikh, Sekhar, & Thomas, 2008):

$$Sensitivity = \frac{TP}{TP + FN} \quad (2)$$

$$Specificity = \frac{TN}{TN + FP} \quad (3)$$

Sensitivity and specificity take values between 0 and 1. The closer to 1 the sensitivity and specificity of a given class are, the better the classification performance of the model.

3. Results and discussion

In Table 1 the physical characteristics of the sample set of tubers are summarized, such as the skin and flesh color and the weight. Also the resistance against internal bruising according to the European cultivated potato database is reported (SASA, 2015).

Once all the peeled tubers were photographed we observed that 15.9% of the tubers subjected to impacts had not developed any blackspot damage, while 12.7% of the healthy tubers presented some kind of damage in the scanned area including blackspot (70.5%) and internal fissures and crushing (29.5%), according to the classification system for impacts made by Baritelle et al. (2000). An RGB image of a potato sample 24 h after impact, before (a) and after peeling (b) is shown in Fig. 4. In this figure, it can clearly be observed that before removing the skin (Fig. 4a) in some tubers it is not possible to visually detect any bruise, while the blackspot can be clearly seen after peeling them (Fig. 4b).

In Fig. 5a&b the mean + standard deviation reflectance spectra obtained from the Vis-NIR and SWIR hyperspectral imaging systems are shown. It can be seen that the variation is higher in the SWIR hyperspectral range. In Fig. 6, the mean spectra of the different groups obtained with both setups are plotted together in order to investigate any possible differences between the measurement times. From Fig. 6a it can be seen that the mean spectra for the different times after bruising overlap in the Vis-NIR spectral range, while the mean spectrum of the healthy group can be distinguished from the rest. Compared to the other groups, the healthy tissue has the highest reflectance from 600 nm to 900 nm. This is in accordance with Porteous, Muir, and Wastie (1981) who obtained a notably reduced reflectance in areas of potato with brown lesions compared to normal tissue from the 600–900 nm spectral range. Same behaviour was observed in apples by Xing et al. (2007) where the absorption by water was initially high (500–800 nm) in a bruised area as the water was set free from the cells, but after some time the absorption decreased because that water was lost through evaporation. Moreover, Fig. 6a shows a higher reflectance of the healthy group at the water peak around 970 nm which could also be attributed to water loss from the bruised tissue.

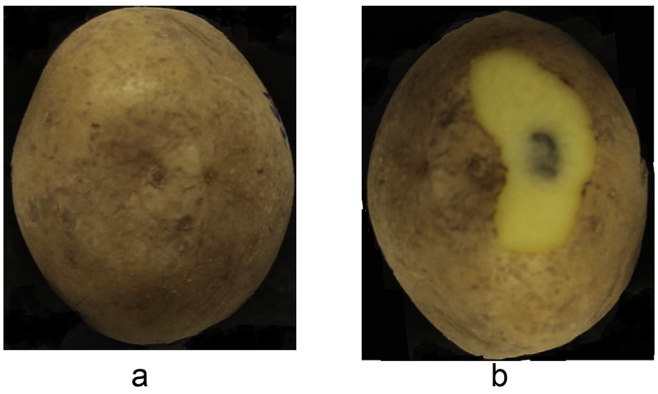

Fig. 4. One sample photographed 24 h after bruising (a) before and (b) after peeling.

In Fig. 6a no clear temporal hierarchy in the reflectance spectra for the different groups after bruising can be noticed. The 24 h group shows the lowest reflectance in the region between 600 and 900 nm.

The mean spectra of the different groups in the SWIR region (Fig. 6b) appeared overlapped too. Here, there is also no clear correlation between the spectra and the time after bruising. It can be observed from the figure that the mean spectra of the healthy and 1 h groups are overlapped along the wavelength range and separated from the rest, especially between 1400 and 1700 nm where they show lower reflectance than the rest. As the 1400 nm region is characteristic for absorption by water, Fig. 6b suggests that the water content in potatoes from the healthy and 1 h groups was higher than in bruised (blackspot affected) ones. This could either be due to a loss of water as a consequence of the bruise or the set of samples subjected to impacts had lower content of water than the healthy set at the beginning of the study. A positive correlation between blackspot and specific gravity has been reported by several researchers. Authors found that potatoes with a higher

Table 1
Characteristics of the potato samples.

Cultivars	Number of samples (n)	Skin color	Flesh color	Resistance to internal bruising	Weight (g)
Hermes	109	White to yellow	Yellow	Very low	103–212
Bintje	44	White to yellow	Light yellow	High	148–338
Magnum	35	White to yellow	White	Not reported	112–315

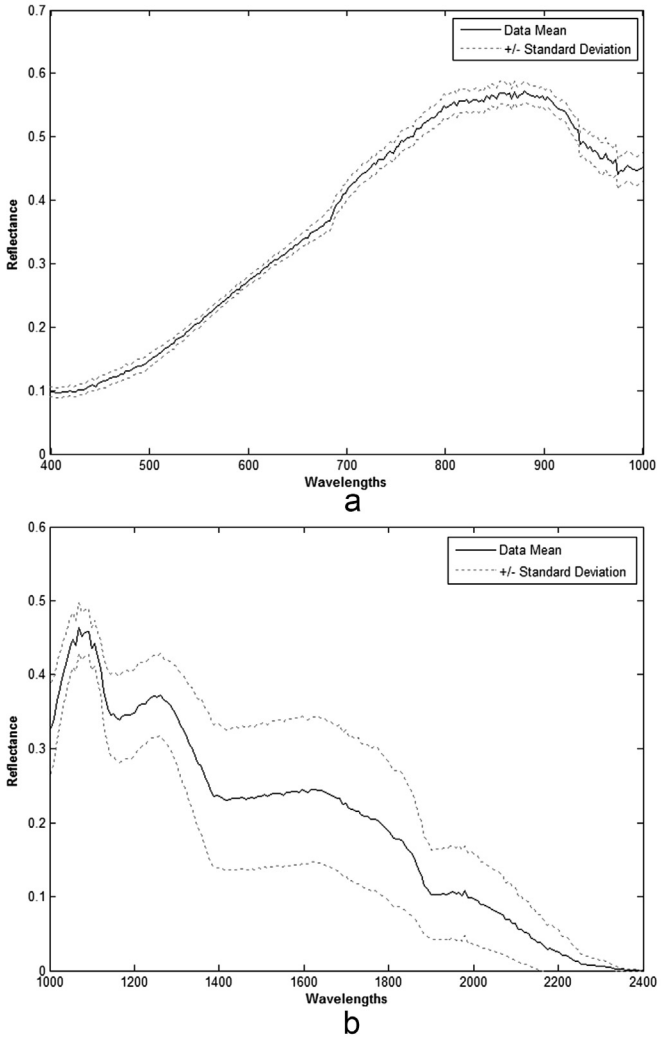

Fig. 5. Mean ± standard deviation reflectance spectra of potato samples for Vis-NIR (a) and SWIR (b) spectral range.

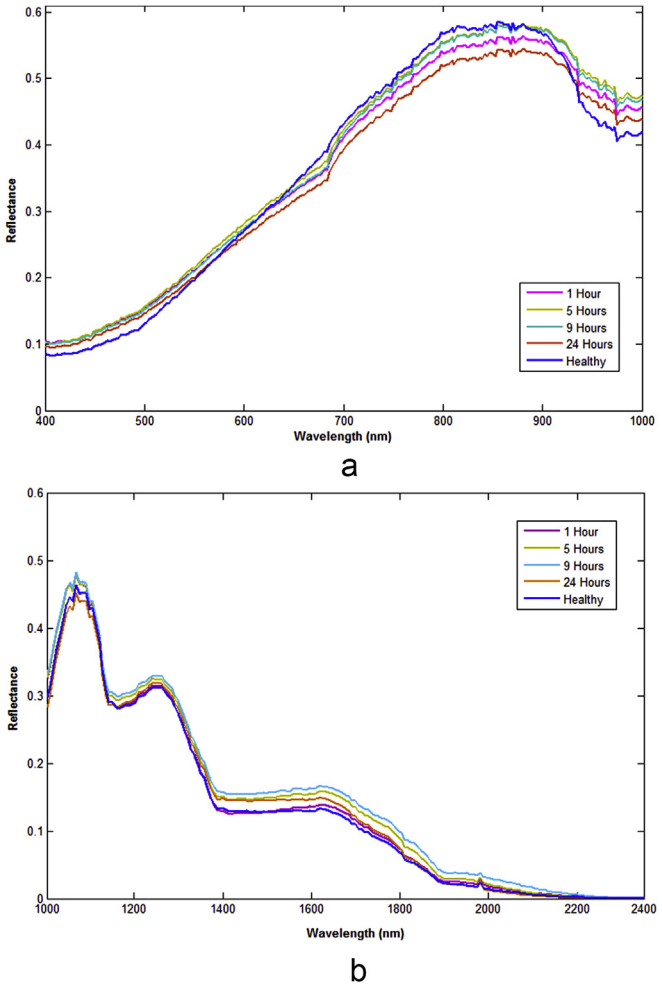

Fig. 6. Mean spectra for each group of samples for Vis-NIR (a) and SWIR (b) spectral range.

specific gravity were more susceptible to blackspot (Scudder, 1951; Zhu et al., 2010). The higher the specific gravity of the samples, the lower the water content (Hegney, 2001). Similarly, Workman and Holm (1984) reported a positive correlation between blackspot susceptibility and dry matter content. However, they only observed this for recently harvested tubers, while such correlation was not observed for long store tubers.

3.1. Masking

The sequential procedure for image segmentation is displayed in Fig. 7. In Fig. 7a, a sample is plotted at those wavelengths with the highest intensity for both Vis-NIR and SWIR setups. Fig. 7b shows a binary image of the whole potato including the saturated pixels for Vis-NIR and SWIR hyperspectral ranges while Fig. 7c shows a binary image of saturated pixels after applying the high mask. Finally, Fig. 7d shows the isolated potato after subtracting saturated pixels from the first binary image (Fig. 7b) to produce a mask containing only the no-saturated areas of the potato in a black background. As mentioned before, bruises were facing the same way for both Vis-NIR and SWIR hyperspectral measurements, but samples were slightly moved between measurements and this is the reason why they may not look exactly the same.

3.2. PCA

A PCA was carried out in order to explore the spectral differences between the two groups of samples. Moreover, all combinations of the pre-processing techniques formerly described were studied. Six PCs were selected for the Vis-NIR range explaining 98.54% of the variance, while seven PCs were chosen in the SWIR range, representing 96.52% of the variance. In Fig. 8a, PC 1 is plotted *versus* PC 4 in the Vis-NIR spectral range, showing that all healthy samples present negative values in this PC 4 and could be separated along it. Although PC 1 and PC 2 represented the main part of the data variance (91.55 and 3.31%, respectively), no class separation was observed by plotting those PCs together (not shown).

In Fig. 8b, the score plot of PC 1 against PC 6 is shown, from which it is observed that PC 6 plays an important role in separating the Healthy from the 24 h group. This result is similar than the one in the previous plot, in which even though PC 1 and PC 2 represented the main part of the data variance (41.44 and 29.17%, respectively), no group separation was observed by plotting these two (not shown).

3.3. SIMCA

SIMCA models were assessed in terms of correctly classified (CC) samples and sensitivity and specificity of each Class. Only best

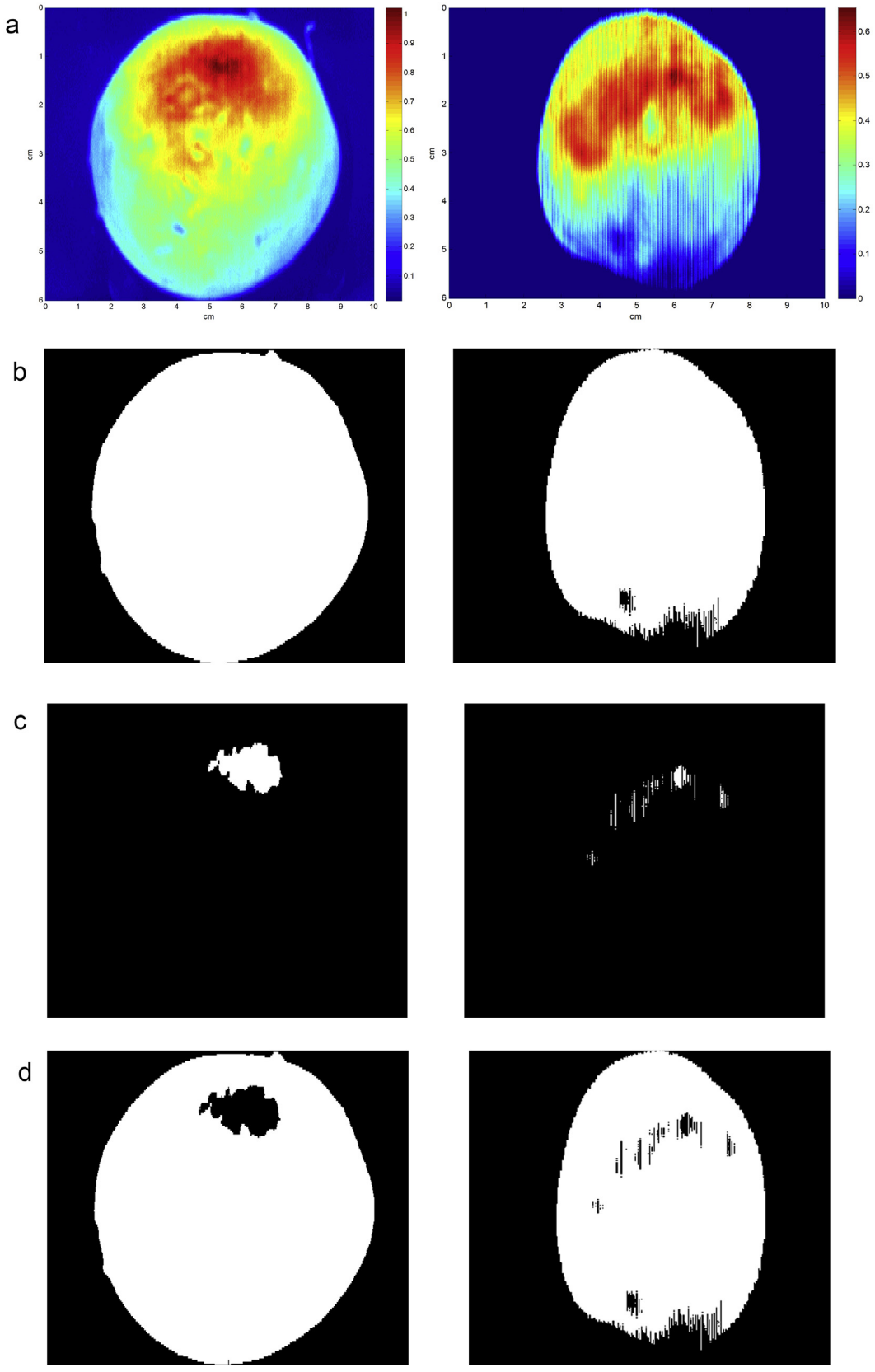

Fig. 7. Low and high masks of a potato sample for Vis–NIR and SWIR images, (a) images in bands 854 and 1106 nm for Vis–NIR and SWIR, respectively, were used to select a threshold, (b) images after applying the low mask, (c) images after applying the high mask, (d) images after applying the low and high masks for Vis–NIR and SWIR setups.

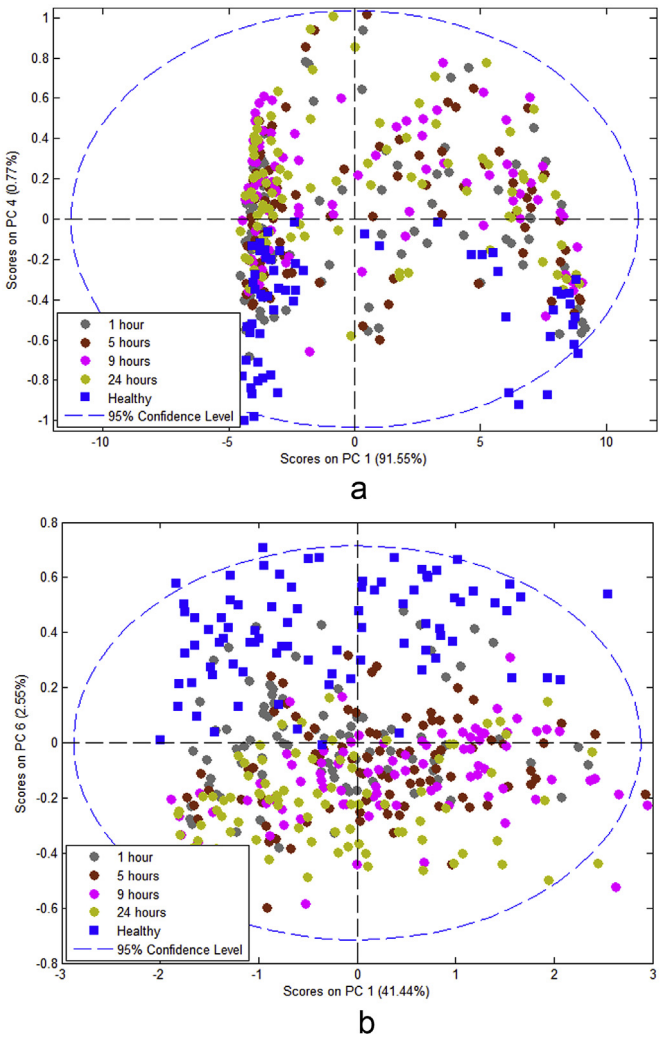

Fig. 8. Score plot of PC1 *versus* PC4 for bruise detection in the Vis-NIR (a) and PC1 *versus* PC 6 in SWIR (b) images for D2 + SNV pre-processing technique.

results corresponding to the combination of smoothing, second derivative, SNV and mean centre pre-processing technique are displayed. The use of that combination resulted in a notable improvement with respect to no pre-treatment at all in the Vis-NIR range, with a classification rate 35.7% higher. An improvement of 12.71% was achieved in comparison to the use of SG + 1D + SNV + MC, and similarly a higher classification rate of 14.76% was obtained compared to the results when SG + either SNV or MSC + MC pre-processing was used.

In Table 2 the % CC samples for the two classes are summarized for both hyperspectral setups. A total of 92.59% healthy samples and 75% bruised in the test set were correctly classified based on the Vis-NIR spectra. From these 25% of bruised samples wrongly classified as healthy, 56.86% corresponded to 1 h group, 19.61% to the 5 h group, 11.76% to the 9 h group and the rest were samples from the 24 h group (11.76%).

Table 2
The % CC tubers by hyperspectral imaging in SIMCA and PLS-DA classification models.

Classes	SIMCA				PLS-DA			
	Vis-NIR		SWIR		Vis-NIR		SWIR	
	Train	Test	Train	Test	Train	Test	Train	Test
Healthy	98.48	**92.59**	100	**100**	96.97	**96.29**	100	**100**
Bruised	80.68	**75**	81.12	**77.23**	95.07	**94.64**	97.63	**97.12**

Values in bold correspond to the percentage of correctly classified samples in the test set.

In the SWIR spectral range a remarkable improvement of 32.5% was achieved by the combination of SG + D2 + SNV + MC in comparison to the model obtained when no pre-processing was applied. Comparing this combination with the use of SG + D1 + SNV + MC, an improvement of 19.38% of samples correctly classified was obtained. Finally, classification rates between 19 and 25% higher were achieved in contrast to the results found when using a combination of SG + SNV or MSC + MC.

A better classification rate was achieved in the SWIR spectral range with 100% and 77.23% CC tubers in Healthy and Bruised Classes, respectively. From the bruised samples that were incorrectly classified as healthy, 65.22% corresponded to the 1 h group, 30.43% were samples from the 5 h group and the rest (4.35%) corresponded to samples analyzed 9 h after bruising. No misclassifications were observed for the samples which had been measured 24 h after bruising.

The detection of internal damage in fruit and vegetables by applying SIMCA was also investigated by other authors. Pholpho, Pathaveerat, and Sirisomboon (2011), studied the capability of visible spectroscopy to detect bruised longan fruits. They were able to correctly classify 86% of them when applying SIMCA. Liu, Chen, Wang, Chan, and Kim (2006), also obtained very good results by the use of a hyperspectral imaging in the 447–951 nm range, coupled with SIMCA for the detection of chilling injury in cucumbers with almost 92% CC samples.

Regarding potatoes, Gao et al. (2013) conducted a study for the detection of black heart in raw tubers by the use of transmission hyperspectral imaging. They reported an accurate identification of black heart of 100% in the range between 400 nm and 1000 nm. More recently, Zhou, Zeng, Li, and Zheng (2015) also investigated the identification of black heart in potatoes using Vis/NIR transmittance spectroscopy combined with PLS-DA in the 513–850 nm region. They achieved overall classification rates above 96% in the validation set.

In Table 3, the sensitivity and specificity values for both spectral ranges with SG + D2 + SNV + MC pre-processing technique are summarized. A total of 9 PCs were selected for both classes (Healthy and Bruised) in the Vis-NIR explaining 99.45 and 99.35% of the variance, respectively. Besides, 5 and 6 PCs were chosen for Healthy and Bruised Classes explaining 96.17 and 96.44% of the variance respectively for the SWIR setup. As shown in Table 3, the sensitivity value of Healthy Class in the Vis-NIR was higher than that of Bruised Class and close to 100% in both training and test sets. In comparison, higher sensitivity and specificity values were obtained in the SWIR spectral range for both classes. These results suggest that SIMCA allows to discriminate healthy from bruised potato tubers based on the acquired hyperspectral images.

3.4. PLS-DA

PLS-DA models were also evaluated in terms of % CC samples and sensitivity and specificity of each group. In Table 2 the % CC samples for each of Class are summarized for training and test sets for both spectral ranges. Only the best results are shown, which correspond to the smoothing, second derivative, SNV and mean centre pre-processing technique. By the use of the former combination of pre-processing techniques, the classification results for the Vis-NIR data improved with 13.36% compared to the case without pre-processing. On the other hand, similar classification results were obtained through combination of SG, either a

Table 3
The obtained sensitivity and specificity results by SIMCA and PLS-DA models.

Models	Setup	Vis-NIR					SWIR				
	Classes	PC/LV	Sensitivity		Specificity		PC/LV	Sensitivity		Specificity	
			Train	Test	Train	Test		Train	Test	Train	Test
SIMCA	Healthy	9	0.984	**0.925**	0.806	**0.750**	5	1	**1**	0.811	**0.772**
	Bruised	9	0.806	**0.750**	0.984	**0.925**	6	0.811	**0.772**	1	**1**
PLS-DA	Healthy	6	0.969	**0.962**	0.950	**0.946**	4	1	**1**	0.976	**0.971**
	Bruised		0.950	**0.946**	0.969	**0.962**		0.976	**0.971**	1	**1**

scattering technique or a first derivative and MC compared to the use of SG + D2 + SNV + MC, improving the latter by 0.5%.

In the Vis-NIR spectral range the mean classification success in terms of prediction was above 94%. From the 5.36% of bruised samples which were wrongly classified as healthy, 66.67% of the samples corresponded to the 1 h group, 16.67% to the 5 h group and another 16.67% to the 9 h group. These results suggest that by the use of Vis-NIR hyperspectral imaging and PLS-DA classification it is possible to accurately discriminate healthy tubers from bruised potatoes 24 h after bruising, while there is some misclassification for shorter times after impact.

In the SWIR spectral range the best results were also obtained through combination of SG + D2 + SNV + MC, improving by 8.05% compared to the models on the original data. Likewise, comparing the former combination of pre-processing to the use of SG + D1 + SNV + MC, a 6.7% better classification rate was achieved. Moreover, between 8 and 11% more samples were correctly classified with respect to the combination of SG + SNV or MSC + MC.

In comparison with the results obtained for the Vis-NIR data, better classification rate of healthy samples was obtained in the SWIR range, where 100% of the tubers were correctly classified. On the other hand, 97.12% of the tubers from the bruised group were correctly identified as bruised. It should be noted that all the misclassified samples corresponded to the 1 h group, which suggests that hyperspectral imaging in the SWIR range in combination with PLS-DA allows the detection of bruises a few hours after bruising.

Similar classification results were reported by Gowen et al. (2008) using hyperspectral imaging and PCA for bruise damage detection in mushrooms. Additionally, as stated previously, bruise detection in apples has been widely investigated. Several authors have reported correct classification rates above 77% by using different spectral regions (Lu, 2003; Xing & De Baerdemaeker, 2005; Xing et al., 2007). Also, ElMasry et al. (2008) were able to detect bruises in apple as early as 1 h after bruising. Non-destructive detection of bruises in potatoes has been less extensively investigated than in apples. However, Dacal-Nieto et al. (2011b) studied the application of hyperspectral imaging and chemometrics for determining the presence of hollow heart, an internal defect in potato tubers, achieving a correct classification rate of 89% for healthy and affected tubers. Moreover, Jin, Li, Liao, Yu, and Viray (2009) were able to classify more than 91% of tubers showing external defects by using computer vision technology.

In Table 3 the sensitivity and specificity values are summarized for the PLS-DA models. A total of 6 and 4 LVs were used to build the PLS-DA model explaining 97.54 and 83.88% of the spectral variance in Vis-NIR and SWIR spectral ranges, respectively. Sensitivity and specificity values obtained for Classes 1 and 2 were above 94% in both training and test sets for the Vis-NIR range. From Table 3 it can be seen that the sensitivity values for Class 1 (healthy) were 100% for both training and test sets in the SWIR spectral range. Furthermore, sensitivity values above 97% were obtained for Class 2 (bruised) in both training and test sets. The fact that the PLS-DA model for the Vis-NIR data performs worse in predicting the Y-variance even though it captures more spectral variance suggests some kind of overfitting.

These results suggest that the combination of hyperspectral imaging techniques and PLS-DA allows to accurately discriminate healthy from bruised potatoes. Moreover, blackspot affected tubers could be identified within 5 h after bruising by means of SWIR hyperspectral imaging.

In order to compare both classification methods, it should be mentioned that PLS-DA achieved more accurate results for classification of both classes in the Vis-NIR and SWIR spectral ranges. In Fig. 9 the regression coefficients are shown for the PLS-DA model built for the Vis-NIR (Fig. 9a) and SWIR (Fig. 9b) range after using SG + D2 + SNV + MC pre-processing. As shown in Fig. 9a, the

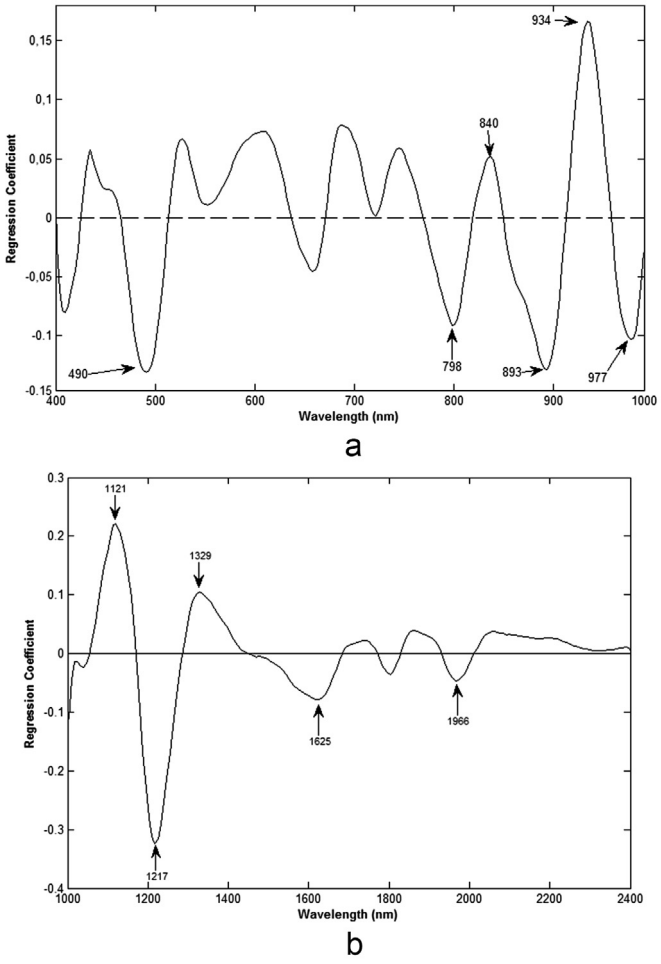

Fig. 9. Regression coefficient plot for Vis-NIR (a) and SWIR (b) setups using SG + D2+SNV + MC preprocessing.

Table 4
The sensitivity, specificity and % CC results by the pixel based PLS-DA model.

Setup		Classes	n	LV	Sensitivity	Specificity	% CC
Vis-NIR	Train	Healthy/Bruised	463,995	5	0.967	0.912	93.92
	Test	Healthy/Bruised	178,560		**0.912**	**0.898**	**90.82**
SWIR	Train	Healthy/Bruised	269,938	5	0.914	0.930	92.16
	Test	Healthy/Bruised	109,814		**0.947**	**0.927**	**93.71**

important wavelengths are located along the entire 400 nm–1000 nm spectral region. Based on Fig. 9a, the most informative wavelengths for the PLS-DA model are 490, 798, 840, 893, 934 and 977 nm. The absorption at 490 nm may correspond to the yellow color of potatoes and is probably related to the presence of beta-carotene (Du, Fuh, Li, Corkan, & Lindsey, 1998; Penner, 2010). The 934 nm can be associated to the third overtone of CH stretching modes (Osborne, Fearn, & Hindle, 1993), while the 977 nm can be related to the second overtone of OH stretching, normally associated with water content of the samples (Porteous et al., 1981). As shown in Fig. 9b, the important wavelengths in the SWIR spectral region are mainly located at the beginning of the spectral region. According to this figure, the most informative wavelengths for the PLS-DA model are 1121, 1217, 1329, 1625 and 1966 nm. The 1121 nm, 1217 nm and 1329 nm bands could be assigned to the influence of CH stretching modes (Osborne et al., 1993). This could be a result of the formation of intermediates during the complete conversion from tyrosine to melanin that occurs in the course of blackspot formation as a results of the harvesting and managing of tubers. That blackspot formation occurs due to the oxidation of the polyphenols present in the tubers. The initial reaction by polyphenol oxidase catalyses the oxidation of *o*-diphenols to produce *o*-quinones, that are highly reactive and suffer a succession of non-enzymatic reactions to produce melanin pigments responsible for potato browning (Massey, 1952). The 1966 nm is associated with water absorptions bands due to second and first overtones of OH stretching and OH combination bands. This may be associated with water loss from the tissue in and around the bruised zone (Porteous et al., 1981).

3.4.1. Mapping of the affected area

In Table 4 the sensitivity and specificity values and the %CC samples for the pixel based PLS-DA model with SG + MC pre-processing technique are shown. A total of 5 LVs were used to build the model in both Vis-NIR and SWIR spectral ranges explaining respectively 99.81 and 98.89% of the variance. Although 5 tubers (5 hypercubes) were individually used as a test set, only averaged results are presented here. Slightly better results were obtained in the SWIR spectral range in terms of % CC samples and sensitivity and specificity. In any case, % CC pixels above 90% were obtained in both spectral ranges with high sensitivity and specificity values. It should be mentioned that the labelling of the images was quite hard, so part of the misclassifications may be due to incorrect labelling of the hypercubes.

In Fig. 10a the sequence for blackspot detection from the acquired hypercubes is schematically illustrated. The first image on the left corresponds to the original hypercube of a sample measured with the Vis-NIR spectral range 24 h after impact in which the bruised mask is represented only by its edges. We can see that this blackspot area is not easily identified and could be easily confused with any other mark present on the tuber. However, the impact procedure was carried out in a controlled way that allowed us to know exactly where the bruises should be located. The second figure on the left corresponds to the segmented hyperspectral cube of the entire sample. The third figure on the left corresponds to the mapping of the bruised area, where we can see some misclassified pixels. However, the blackspot area in the centre is correctly identified. The last figure shows the segmented hyperspectral cube with the mapping of the bruised area and the

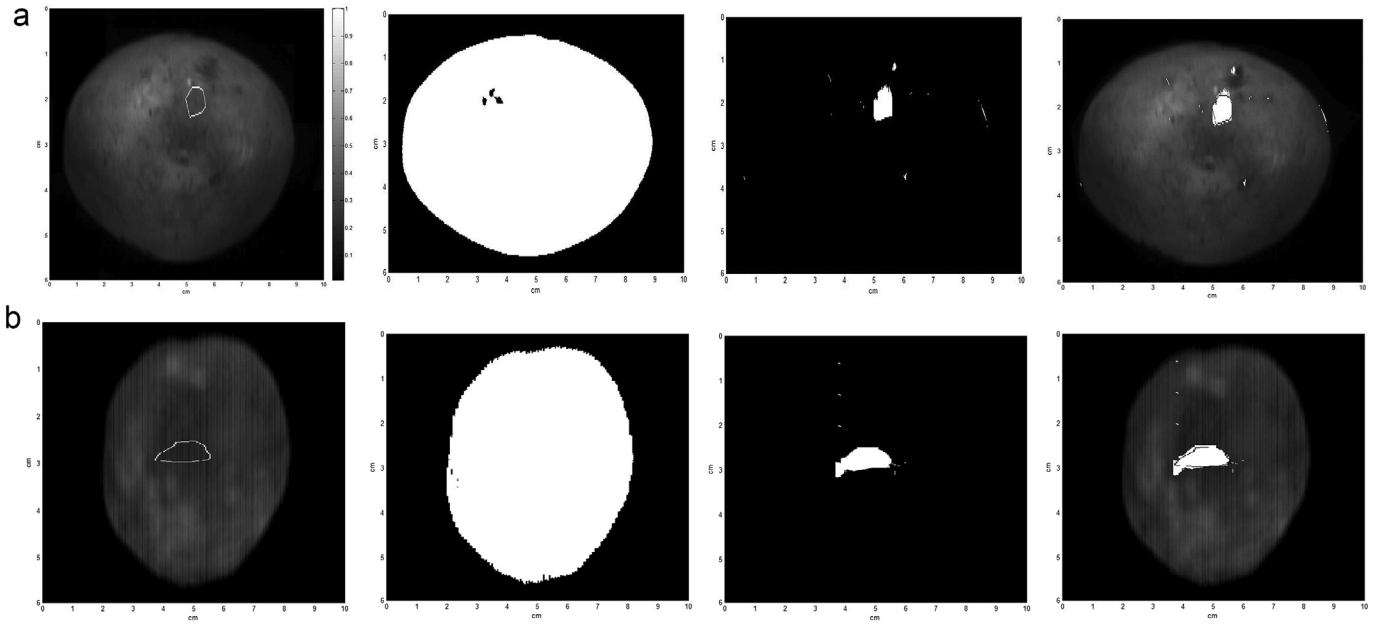

Fig. 10. An example of the operation of the blackspot detection system in the Vis-NIR (a) and SWIR (b) spectral range. From left to right: original hypercube with the edges of the bruised mask, segmented hyperspectral cube, mapping of the bruised area, segmented hyperspectral cube with the mapping of the bruised area and the edges of the bruised mask.

edges of the bruised mask. In Fig. 10b the operation of the blackspot detection system in the SWIR spectral range is illustrated as well. The first image on the left corresponds to the original hypercube and the edges of the bruised mask of a sample measured 24 h after impact, there is a bruised area located in the centre. The second image on the left shows the segmented hyperspectral cube of the tuber. In the third figure, the mapping of the bruised area is shown. Similar to the Vis-NIR spectral range, there are some misclassified pixels, while the blackspot is identified well. Finally, the last figure shows the segmented hyperspectral cube with the mapping of the blackspot affected area and the edges of the bruised mask in order to compare the results.

As commented previously, there are no records of the application of hyperspectral imaging systems for the detection of blackspot in potatoes as far as we are concerned.

4. Conclusion

The results obtained in this study suggest that it is possible to identify raw potatoes affected by blackspot by combining hyperspectral imaging and chemometric techniques. The correct classification rate was between 2 and 7% higher for the SWIR range (1000–2500 nm) than for the Vis-NIR range (400–1000 nm) for Classes 1 and 2 for both SIMCA and PLS-DA discrimination methods. Furthermore, it was observed that more accurate discrimination of healthy and bruised tubers was achieved by applying PLS-DA to SWIR hyperspectral imaging data where all samples belonging to 5, 9 and 24 h groups and the healthy set were correctly classified into their corresponding group. Therefore, it can be concluded that SWIR coupled with PLS-DA is able to accurately identify early bruises in potatoes within 5 h after bruising.

Moreover, in this study, we were able to map the areas affected by blackspot in a set of potato samples with a pixel classification accuracy above 93% when using the SWIR spectral range.

According to these results, the use of SWIR hyperspectral imaging coupled with PLS-DA to detect blackspot in raw potatoes has potential for on-line quality control of tubers in industry. The application of NIR hyperspectral imaging could enable the development of a fast, reliable and non-destructive method for internal damage detection of potatoes avoiding the commercialization of affected tubers. This would be beneficial to both potato industry and consumers. However, it should be mentioned that prior to the implementation of this system in the potato industry, those results must be validated on a larger sample set covering a wide range of potato varieties grown in different areas and under different conditions.

Acknowledgments

The funding of this work has been covered by the Universidad Pública de Navarra through the concession of both a predoctoral research grant (Res. 1753/2012) and a mobility grant (Res. 1506/2013), by the National Institute for Agricultural and Food Research and Technology (INIA) project: “Mejora genética de la patata: caracterización reológica y por tecnología NIRS del material.” RTA2013-00006-C03-03, and by the Agency for Innovation by Science and Technology in Flanders (IWT) through the Chameleon (SB-100021) project. The authors would also like to thank the Basque Institute for Agricultural Research and Development (Neiker Tecnalia) for supplying some of the samples used in this study. Janos Keresztes and Mohammad Goodarzi have been funded respectively as PhD student and postdoctoral researcher on the IWT Chameleon project (SB-100021).

References

Ballabio, D., & Todeschini, R. (2009). *Multivariate classification for qualitative analysis* (pp. 83–104). Burlington, MA, USA: Elsevier.

Barbin, D. F., ElMasry, G., Sun, D. W., & Allen, P. (2012). Predicting quality and sensory attributes of pork using near-infrared hyperspectral imaging. *Analytica Chimica Acta, 719*, 30–42.

Baritelle, A., Hyde, G., Thornton, R., & Bajema, R. (2000). A classification system for impact-related defects in potato tubers. *American Journal of Potato Research, 77*(3), 143–148.

Barker, M., & Rayens, W. (2003). Partial least squares for discrimination. *Journal of Chemometrics, 17*(3), 166–173.

Boeriu, C., Yuksel, D., Van der Vuurst de Vries, R., Stolle-Smits, T., & Van Dijk, C. (1998). Correlation between near infrared spectra and texture profiling of steam cooked potatoes. *Journal of Near Infrared Spectroscopy, 6*(A), 291–297.

Brown, C., Culley, D., Yang, C.-P., Durst, R., & Wrolstad, R. (2005). Variation of anthocyanin and carotenoid contents and associated antioxidant values in potato breeding lines. *Journal of the American Society for Horticultural Science, 130*(2), 174–180.

Burger, J., & Geladi, P. (2007). Spectral pre-treatments of hyperspectral near infrared images: analysis of diffuse reflectance scattering. *Journal of Near Infrared Spectroscopy, 15*(1), 29–38.

Casale, M., Casolino, C., Oliveri, P., & Forina, M. (2010). The potential of coupling information using three analytical techniques for identifying the geographical origin of Liguria extra virgin olive oil. *Food chemistry, 118*(1), 163–170.

Dacal-Nieto, A., Formella, A., Carrión, P., Vazquez-Fernandez, E., & Fernández-Delgado, M. (2011a). Common scab detection on potatoes using an infrared hyperspectral imaging system. In *Paper presented at the Image Analysis and Processing–ICIAP 2011* (Vol. 6979, pp. 303–312).

Dacal-Nieto, A., Formella, A., Carrión, P., Vazquez-Fernandez, E., & Fernández-Delgado, M. (2011b). Non-destructive detection of hollow heart in potatoes using hyperspectral imaging. In *Paper presented at the 14th Computer Analysis of Images and Patterns 2011* (Vol. 6855, pp. 180–187).

Dean, B., Jackowiak, N., Nagle, M., Pavek, J., & Corsini, D. (1993). Blackspot pigment development of resistant and susceptible *Solanum tuberosum* L. genotypes at harvest and during storage measured by three methods of evaluation. *American Potato Journal, 70*(3), 201–217.

Dhanoa, M., Lister, S., Sanderson, R., & Barnes, R. (1995). The link between multiplicative scatter correction (MSC) and standard normal variate (SNV) transformations of NIR spectra. *Journal of Near Infrared Spectroscopy, 2*(1), 43–47.

Du, H., Fuh, R. C. A., Li, J., Corkan, L. A., & Lindsey, J. S. (1998). PhotochemCAD: a computer-aided design and research tool in photochemistry. *Photochemistry and Photobiology, 68*(2), 141–142.

ElMasry, G., Wang, N., Vigneault, C., Qiao, J., & ElSayed, A. (2008). Early detection of apple bruises on different background colors using hyperspectral imaging. *LWT-Food Science and Technology, 41*(2), 337–345.

Evans, S., & Muir, A. (1999). Reflectance spectrophotometry of bruising in potatoes. I. Ultraviolet to near infrared. *International Agrophysics, 13*, 203–210.

FAO. (2014). *Production/Crops*. Retrieved November, 2015, from http://faostat3.fao.org/browse/Q/QC/E.

Fluck, R. C., & Ahmed, E. M. (1973). Impact testing of fruits and vegetables. *Transactions of the ASAE, 16*(4), 0660–0666.

Gao, H., Li, X., Xu, S., Huang, T., Tao, H., & Li, X. (2013). Transmission hyperspectral detection method for weight and black heart of potato. *Transactions of the Chinese Society of Agricultural Engineering, 29*(15), 279–285.

Gowen, A., O'donnell, C., Taghizadeh, M., Cullen, P., Frias, J., & Downey, G. (2008). Hyperspectral imaging combined with principal component analysis for bruise damage detection on white mushrooms (Agaricus bisporus). *Journal of Chemometrics, 22*(3–4), 259–267.

Hägg, M., Häkkinen, U., Kumpulainen, J., Ahvenainen, R., & Hurme, E. (1998). Effects of preparation procedures, packaging and storage on nutrient retention in peeled potatoes. *Journal of the Science of Food and Agriculture, 77*(4), 519–526.

Hegney, M. (2001). *Specific gravity of potatoes*. Farmnote/Western Australian Department of Agriculture.

Hesen, J., & Kroesbergen, E. (1960). Mechanical damage to potatoes I. *Potato Research, 3*(1), 30–46.

Höskuldsson, A. (1988). PLS regression methods. *Journal of Chemometrics, 2*(3), 211–228.

Jack, K., Dessureault, M., & Prasad, R. (2013). *Post-harvest life of organic potatoes* (Vancouver, Canada).

Jin, J., Li, J., Liao, G., Yu, X., & Viray, L. C. C. (2009). Methodology for potatoes defects detection with computer vision. In *Paper presented at the international symposium on information processing, Huangshan*.

Kamruzzaman, M., Barbin, D., ElMasry, G., Sun, D. W., & Allen, P. (2012). Potential of hyperspectral imaging and pattern recognition for categorization and authentication of red meat. *Innovative Food Science & Emerging Technologies, 16*, 316–325.

Kennard, R. W., & Stone, L. A. (1969). Computer aided design of experiments. *Technometrics, 11*(1), 137–148.

Kleinschmidt, G., & Thornton, M. (1991). *Bruise-free potatoes: Our goal*. Bulletin-Idaho Agricultural Experiment Station (USA). no. 725.

Kotikova, Z., Hejtmankova, A., Lachman, J., Hamouz, K., Trnkova, E., & Dvorak, P. (2007). Effect of selected factors on total carotenoid content in potato tubers (*Solanum tuberosum L.*). *Plant Soil and Environment, 53*(8), 355.

Liu, Y., Chen, Y., Wang, C., Chan, D., & Kim, M. (2006). Development of hyperspectral imaging technique for the detection of chilling injury in cucumbers; spectral and image analysis. *Applied Engineering in Agriculture, 22*(1), 101.
López, A., Arazuri, S., García, I., Mangado, J., & Jarén, C. (2013). A review of the application of near-infrared spectroscopy for the analysis of potatoes. *Journal of Agricultural and Food Chemistry, 61*(23), 5413–5424.
Lu, R. (2003). Detection of bruises on apples using near-infrared hyperspectral imaging. *Transactions-American Society of Agricultural Engineers, 46*(2), 523–530.
Martens, H., & Naes, T. (1989). *Multivariate calibration*. John Wiley & Sons.
Massart, D. L., Vandeginste, B., Deming, S., Michotte, Y., & Kaufman, L. (1988). *Chemometrics: A textbook* (Vol. 2). Amsterdam: Elsevier.
Massey, P. H. (1952). *Field and storage experiments on internal black spot of potatoes*. Cornell Univ. (June).
Mathew, R., & Hyde, G. (1997). Potato impact damage thresholds. *Transactions of the ASAE, 40*(3), 705–709.
O'Leary, A. G., & Iritani, W. (1969). Potato bruise detection. *American Journal of Potato Research, 46*(9), 352–354.
Osborne, B., Fearn, T., & Hindle, P. (1993). Introduction. In D. Brownin (Ed.), *Practical NIR spectroscopy with applications in food and beverage analysis* (2nd ed., p. 227). Harlow: Longman Scientific and Technical.
Parikh, R., Mathai, A., Parikh, S., Sekhar, G. C., & Thomas, R. (2008). Understanding and using sensitivity, specificity and predictive values. *Indian Journal of Ophthalmology, 56*(1), 45.
Penner, M. H. (2010). Ultraviolet, visible, and fluorescence spectroscopy. In S. S. Nielsen (Ed.), *Food analysis* (pp. 387–405). Springer.
Peters, R. (1996). Damage of potato tubers, a review. *Potato Research, 39*(4), 479–484.
Pholpho, T., Pathaveerat, S., & Sirisomboon, P. (2011). Classification of longan fruit bruising using visible spectroscopy. *Journal of Food Engineering, 104*(1), 169–172.
Porteous, R., Muir, A., & Wastie, R. (1981). The identification of diseases and defects in potato tubers from measurements of optical spectral reflectance. *Journal of Agricultural Engineering Research, 26*(2), 151–160.
Rady, A., & Guyer, D. (2015). Rapid and/or nondestructive quality evaluation methods for potatoes: a review. *Computers and Electronics in Agriculture, 117*, 31–48.
Riccioli, C., Pérez-Marín, D., Guerrero-Ginel, J. E., Saeys, W., & Garrido-Varo, A. (2011). Pixel selection for near-infrared chemical imaging (NIR-CI) discrimination between fish and terrestrial animal species in animal protein by-product meals. *Applied Spectroscopy, 65*(7), 771–781.
Rinnan, Å., Berg, F.v.d., & Engelsen, S. B. (2009). Review of the most common pre-processing techniques for near-infrared spectra. *TrAC Trends in Analytical Chemistry, 28*(10), 1201–1222.
SASA. (2015). *The European cultivated potato database*. Retrieved March, 2015, from http://www.europotato.org/menu.php.
Sawyer, R., & Collin, G. (1960). Black spot of potatoes. *American Journal of Potato Research, 37*(4), 115–126.
Scudder, W. T. (1951). *Black spot of potatoes*. Ithaca, N. Y: Cornell Univ.
Thornton, M., & Bohl, W. (1998). *Preventing potato bruise damage* (p. 725). University of Idaho Extension Publications BUL.
Thybo, A. K., Jespersen, S. N., Lærke, P. E., & Stødkilde-Jørgensen, H. J. (2004). Nondestructive detection of internal bruise and spraing disease symptoms in potatoes using magnetic resonance imaging. *Magnetic Resonance Imaging, 22*(9), 1311–1317.
Van Zeebroeck, M., Tijskens, E., Van Liedekerke, P., Deli, V., De Baerdemaeker, J., & Ramon, H. (2003). Determination of the dynamical behaviour of biological materials during impact using a pendulum device. *Journal of Sound and Vibration, 266*(3), 465–480.
Vanderslice, J. T., Higgs, D. J., Hayes, J. M., & Block, G. (1990). Ascorbic acid and dehydroascorbic acid content of foods-as-eaten. *Journal of Food Composition and Analysis, 3*(2), 105–118.
Vidal, M., & Amigo, J. M. (2012). Pre-processing of hyperspectral images. Essential steps before image analysis. *Chemometrics and Intelligent Laboratory Systems, 117*, 138–148.
Wang-Pruski, G., & Nowak, J. (2004). Potato after-cooking darkening. *American Journal of Potato Research, 81*(1), 7–16.
Wold, H. (1966). Estimation of principal components and related models by iterative least squares. *Multivariate Analysis, 1*, 391–420.
Workman, M., & Holm, D. (1984). Potato clone variation in blackspot and soft rot susceptibility, redox potential, ascorbic acid, dry matter and potassium. *American Potato Journal, 61*(12), 723–733.
Xing, J., & De Baerdemaeker, J. (2005). Bruise detection on 'Jonagold' apples using hyperspectral imaging. *Postharvest Biology and Technology, 37*(2), 152–162.
Xing, J., Saeys, W., & De Baerdemaeker, J. (2007). Combination of chemometric tools and image processing for bruise detection on apples. *Computers and Electronics in Agriculture, 56*(1), 1–13.
Zhao, J., Ouyang, Q., Chen, Q., & Wang, J. (2010). Detection of bruise on pear by hyperspectral imaging sensor with different classification algorithms. *Sensor Letters, 8*(4), 570–576.
Zhou, Z., Zeng, S., Li, X., & Zheng, J. (2015). Nondestructive detection of blackheart in potato by visible/near infrared transmittance spectroscopy. *Journal of Spectroscopy, 2015*.
Zhu, X., Li, S., Shan, Y., Zhang, Z., Li, G., Su, D., et al. (2010). Detection of adulterants such as sweeteners materials in honey using near-infrared spectroscopy and chemometrics. *Journal of Food Engineering, 101*(1), 92–97.